IN VIVO VALIDATION OF A ONE-DIMENSIONAL FINITE ELEMENT METHOD FOR SIMULATION-BASED MEDICAL PLANNING FOR CARDIOVASCULAR BYPASS SURGERY

B. N. Steele[1], J. Wan[2], J. P. Ku[3], T. J. R. Hughes[1], C. A.Taylor[1, 4]
[1]Department of Mechanical Engineering, Stanford University, CA, USA
[2]Department of Petroleum Engineering, Stanford University, CA, USA
[3]Department of Electrical Engineering, Stanford University, CA, USA
[4]Department of Surgery, Stanford University, CA, USA

Abstract-**Current practice in vascular surgery utilizes only diagnostic and empirical data to plan treatments, and does not enable quantitative *a priori* prediction of the outcomes of interventions. We have previously described simulation-based medical planning methods to model blood flow in arteries and plan medical treatments based on physiologic models[1, 2]. These methods utilize computationally intensive three-dimensional finite element analysis. We recently described a new method for simulation-based medical planning based on solving one-dimensional equations of blood flow [3]. We demonstrate herein that these one-dimensional methods can be used to simulate blood flow in a porcine thoraco-thoraco bypass and further that predicted flow rates compare favorably to *in vivo* data obtained using cine phase-contrast magnetic resonance imaging in four pigs.**

Keywords **- blood flow, Simulation-Based Medical Planning, one-dimensional analysis methods**

I. INTRODUCTION

At present, vascular surgical planning is based on a diagnostic/empirical paradigm. Surgeons consider each patient's medical condition, expected tolerance to alternate procedures and the anticipated benefit of each treatment. This approach does not enable the *a priori* prediction of the outcomes of alternate interventions for individual patients. The ability to predict changes in blood flow would enable a surgeon to evaluate and rank the treatments in order of efficacy. We have previously described a new approach, Simulation-Based Medical Planning, whereby a physician uses software tools in conjunction with anatomic and physiologic data to design and preoperatively evaluate treatment outcomes [1]. To date, we have solved the time-dependent, three-dimensional equations governing blood flow to obtain detailed data on blood flow distribution, wall shear stress, particle residence time, and flow recirculation. However, these methods are computationally expensive, requiring hours of computation on parallel computers and are not suitable for rapid evaluation of surgical treatments.

Simpler, zero and one-dimensional methods have been used to describe blood flow in arteries and quantify mean flow rate and pressure. These methods include lumped parameter models [4, 5], one-dimensional nonlinear pulse wave propagation methods solved using both frequency domain approaches [6] and numerical methods [7-10]. We have developed a one-dimensional nonlinear pulse wave propagation method using a finite element method [3]. Although one-dimensional analysis methods cannot provide the same level of detail as three-dimensional methods, they may provide adequate information with which to rank treatment outcomes based on mean flow rate and pressure distribution.

A series of animal experiments was performed to test the accuracy of the three-dimensional modeling and flow analysis compared to *in vivo* measurements [11]. Using the same model geometry and flow boundary conditions, we compare the flow waveforms predicted by our one-dimensional method with *in vivo* magnetic resonance data.

II. METHODOLOGY

A. One-Dimensional Method

The one-dimensional equations for the flow of a Newtonian fluid in an impermeable, deforming, elastic domain consist of the continuity equation, a single axial momentum balance equation, a constitutive equation, and suitable initial and boundary conditions. The governing equations are derived in general form by Hughes and Lubliner [12]. The partial differential equations for mass and momentum balance are given by

$$\frac{\partial S}{\partial t}+\frac{\partial Q}{\partial z}=0 \tag{1}$$

$$\frac{\partial Q}{\partial t}+\frac{\partial}{\partial z}\left((1+\delta)\frac{Q^2}{S}\right)+\frac{S}{\rho}\frac{\partial p}{\partial z}=Sf+N\frac{Q}{S}+\nu\frac{\partial^2 Q}{\partial z^2} \tag{2}$$

The primary variables are cross-sectional area S, pressure p, and volumetric flow rate Q. The density of the fluid is given by ρ, the external force by f, and the kinematic viscosity by ν. The variable δ is related to the profile function for the velocity over the cross-sectional area and N is a viscous loss term. We assume that the axial velocity is much greater than the radial velocity components. If we specify the vessel to have a circular cross-section and assume a quadratic flow profile, we obtain

$$\delta=\frac{1}{3} \tag{3}$$

$$N=-8\pi\nu \tag{4}$$

For boundary conditions, we specify the flow rate at the inlet and prescribe a pressure boundary condition at the outlet(s)

$$Q(z,t)=Q(t) \text{ on } \Gamma_{\text{in}}$$

$$p(z,t)=p(t) \text{ on } \Gamma_{\text{out}}$$

We use the constitutive equation described by Olufsen [13].

$$\tilde{p}(S(z,t),z,t)=p_0(z)+\frac{4}{3}Eh\left(1-\sqrt{\frac{S_0(z)}{S(z,t)}}\right) \tag{5}$$

Funding provided by Whitaker Foundation and the American Heart Association, Western States Affiliate

where

$$\frac{Eh}{r_0(z)} = k_1 \exp\left[k_2 r_0(z)\right] + k_3 \tag{6}$$

E is the Young's modulus, h is the wall thickness, and r_0 is the radius at the reference pressure p_0. In the relationship, k_1, k_2, k_3 are derived by a best fit to experimental data and are set to default values of $k_1 = 2\text{x}10^7 g{\cdot}s^{-2}{\cdot}cm^{-1}$, $k_2 = -22.53 cm^{-1}$, and $k_3 = 8.65\text{x}10^5 g{\cdot}s^{-2}{\cdot}cm^{-1}$ [13].

To solve the system of equations, we employ a space-time finite element method including Galerkin Least Squares stabilization and the Discontinuous Galerkin method in time. We use a modified Newton-Raphson technique to solve the resultant nonlinear equations for each time step.

For the one-dimensional theory, the assumptions made for the flow profile are not valid in regions of flow separation such as downstream of stenoses or branches, and the one-dimensional method does not adequately model the pressure losses. The minor loss coefficient, K [14], is defined as a relationship between fluid density ρ, vessel flow rate Q, and cross-sectional area S, and the change in pressure Δp.

$$K = \frac{\Delta p}{\frac{1}{2}\rho\left(\frac{Q}{S}\right)^2} \tag{7}$$

We can incorporate the experimentally determined, dimensionless form, K, into our numerical model through the viscous loss term N. Starting with (2) and assuming a constant flow rate and zero external force. We obtain,

$$\frac{1}{\rho}\frac{dp}{dz} = N\frac{Q}{S^2} \tag{8}$$

If we assume a straight vessel, we can integrate over the length of the vessel and solve for N.

$$N = \frac{\Delta p}{\rho}\frac{S^2}{QL} \tag{9}$$

Combining (7) and (9) we obtain

$$N = \frac{QK}{2L} \tag{10}$$

We implemented the minor loss value for a stenosis model (Fig. 1) developed by Seeley and Young [15]. This model utilizes the area ratio between the stenosed segment and the unobstructed segment prior to the stenosed segment (Fig. 1) to obtain

$$K = 2\left(\frac{K_v}{Re_0} + \frac{K_t}{2}\left[\frac{S_0}{S_1} - 1\right]^2\right)\left(\frac{S_1}{S_0}\right)^2 \tag{11}$$

where Δp is the pressure drop due to the stenosis, Re_0 is the Reynolds number in the unobstructed section, D_0 the unobstructed diameter, and S_0 and S_1 are the cross sectional areas of the unobstructed and stenosed sections respectively. Further,

$$K_v = 32\frac{L}{D_0}\left(\frac{S_0}{S_1}\right)^2 \tag{12}$$

$$K_t = 1.52 \tag{13}$$

represent viscous and turbulent factors with L being the length of the stenosed segment. This K is used in (10) for segments that have a 75% or more reduction in area compared to the distal segment area.

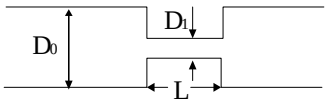

Fig. 1. Stenosis model diagram

We implemented minor loss values for branch junctions of arbitrary angles using a model developed by Gardel [16]. For each branching case of converging flow (Fig. 2) and diverging flow (Fig. 3), minor loss coefficients are computed for the through and branching segment with respect to the combined segment. The branch, through, and combined legs are labeled 1, 2, and 3 respectively.

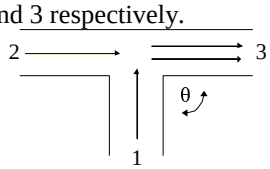

Fig. 2. Converging flow diagram

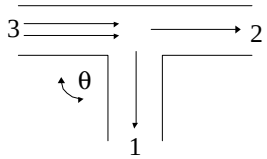

Fig. 3. Diverging flow diagram

Minor loss coefficients are computed for each through, 2, and branch, 1, segment. The coefficient $K_{1,3}$ is the minor loss coefficient for the converging flow branch leg. The subscript indicates flow from 1 into 3. Similarly, $K_{3,2}$ refers to the minor loss coefficient for the through leg of the diverging flow, flow from 3 into 2. The coefficients are expressed in terms of the side branch angle θ, flow ratio $q=q_1/q_3$, and area ratio $a=a_1/a_3$ and are given as

$$K_{1,3} = -0.92(1-q)^2 - q^2\left[1.2\left(\frac{\cos\theta}{a} - 1\right) + 0.8\left(1 - \frac{1}{a^2}\right) - (1-a)\frac{\cos\theta}{a}\right] + (2-a)q(1-q) \tag{14}$$

$$K_{2,3} = 0.03(1-q)^2 - q^2\left[1 - 0.62\left(\frac{\cos\theta}{a} - 1\right) - 0.38(1-a)\right] + (2-a)q(1-q) \tag{15}$$

$$K_{3,1} = 0.95(1-q)^2 + q^2\left(1.3\cot\frac{180-\theta}{2} - 0.3 + \frac{0.4-0.1a}{a^2}\right) + 0.4q(1-q)\left(1 + \frac{1}{a}\right)\cot\frac{180-\theta}{2} \tag{16}$$

$$K_{3,2} = 0.03(1-q)^2 + 0.35q^2 - 0.2q(1-q) \tag{17}$$

These K values are used in (10) for the branch and through segments near a junction.

B. Animal Study

We used data collected from a series of four animal studies. All animal procedures were approved by the university's Institutional Animal Care and Use Committee. In each animal, we created an aortic constriction by tying polyester (Dacron) umbilical tape around the descending thoracic aorta to restrict blood flow and create a diseased state. A polyester (Dacron) graft was attached to the thoracic aorta proximal and distal to the constriction to provide an alternate path for blood flow. This model resembles the anatomy of patients who have been diagnosed with aorto-iliac

disease and have been treated with an aorto-femoral bypass with proximal end-to-side anastomosis. In both cases, blood is divided between the native aorta and the bypass graft and combines downstream of the stenosis.

Anatomic and physiologic data was acquired for each animal using magnetic resonance imaging (MRI). Contrast–enhanced magnetic resonance angiography (CE-MRA) was used to acquire three-dimensional anatomic images of blood vessels, while phase contrast MRI (PC-MRI) was used to collect velocity information at four different locations: the proximal aorta (inlet), the mid-aorta (aorta), the graft, and the distal aorta (outlet) (Fig. 4). Pressure catheters were used to capture the blood pressure proximal and distal to the bypass region [11].

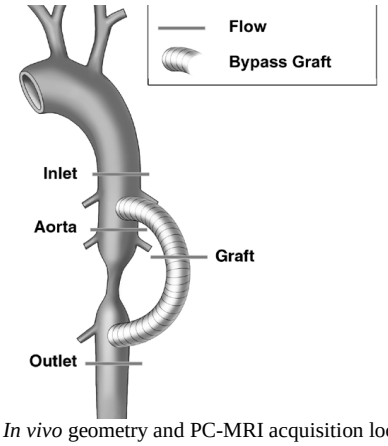

Fig. 4 *In vivo* geometry and PC-MRI acquisition locations

Using a previously described process [17], a geometric model of the thoracic aorta and corresponding bypass was constructed from the CE-MRA data of each animal. The cross sectional profiles of the vessels were approximated with circles for use with the one-dimensional finite element method. A velocity profile was generated from the PC-MRI data at the inlet using custom software [18]. The geometric model, inlet velocity profile, and a constant pressure outlet boundary condition were used to simulate the blood flow for each animal using the one-dimensional finite element method previously described.

III. RESULTS

Flow rate was extracted from both the *in vivo* PC-MRI data and the one-dimensional finite element method at the inlet, aorta, graft, and outlet for each pig. The flow values are plotted for the one-dimensional analyses and PC-MRI for both the aorta and graft for each pig (Fig. 5.)

IV. DISCUSSION

While the one-dimensional model does not match exactly the PC-MRI data, it does provide a good approximation to the flow rate in the aorta and bypass. There are a few sources of error to consider. First, the empirical methods used to model pressure loss for complex geometry were developed under steady flow conditions for rigid vessels and may not be optimal for use in deformable vessels with pulsatile flow. Furthermore, losses associated with curvature are not included. Second, the sum of the measured flow through the

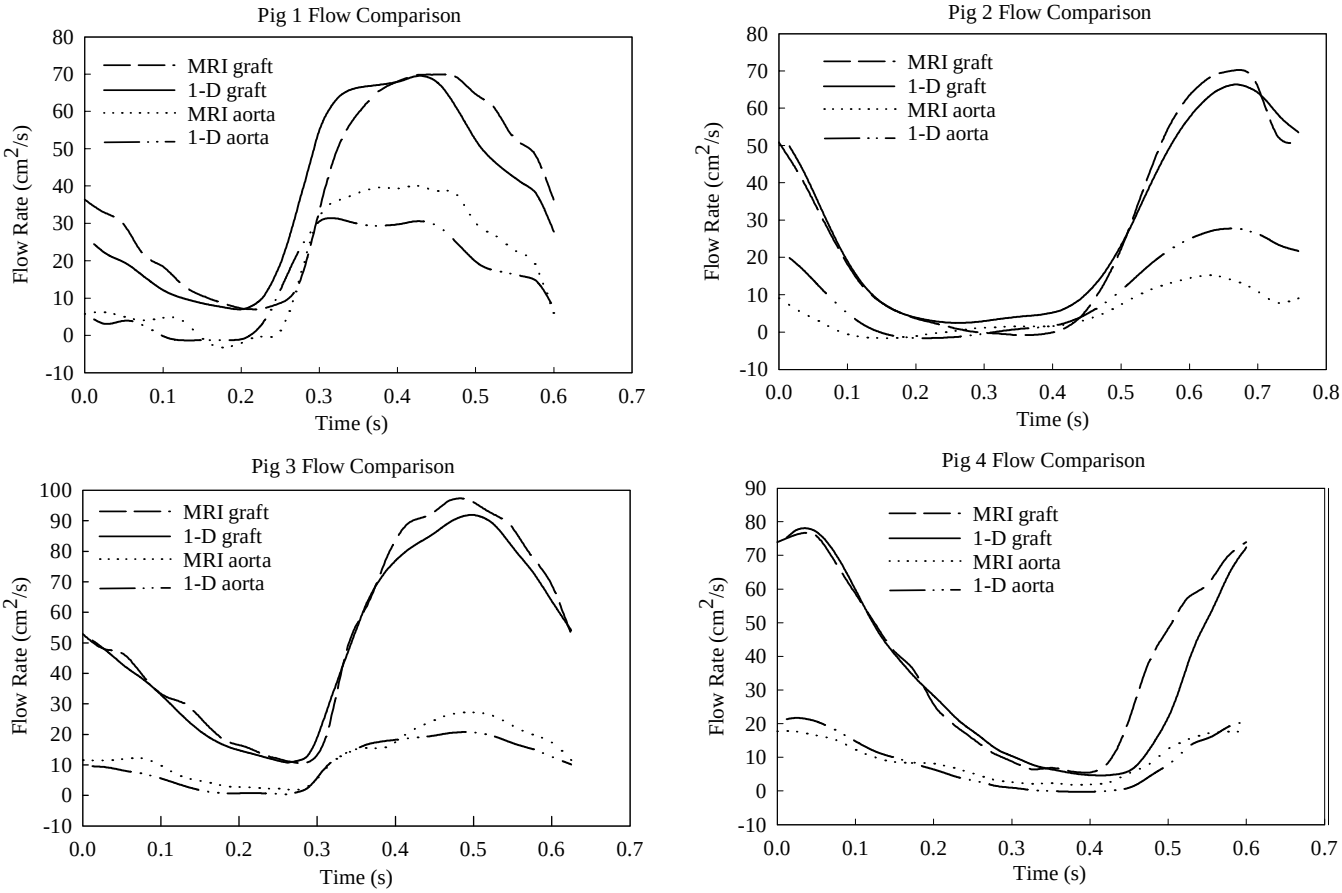

Fig. 5.

in vivo aorta and bypass did not always equal the measured inlet flow. This could be due in part to flow through intercostal arteries in the thoracic aorta in our region of interest, and difficulties in velocity data extraction from PC-MRI. When the mean flow ratios were computed with respect to the combined flow between the aorta and graft, the one-dimensional and PC-MRI values compared favorably (Fig. 6). The greatest discrepancy is with pig 2. The MR sequence used to acquire the velocity data for pig 2 was different from the other test subjects and the respiration was not suspended for pig 2 as it was in the other animals.

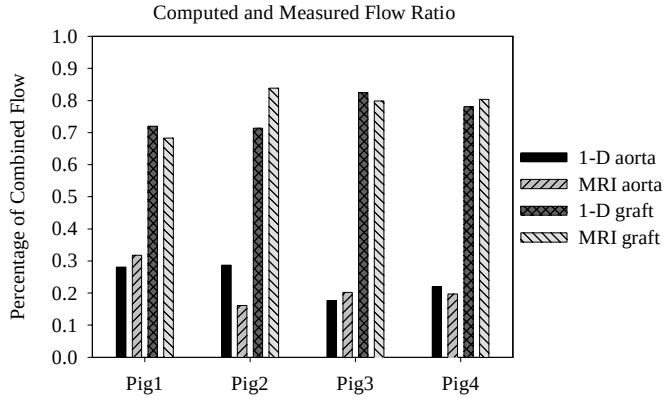

Fig. 6.

V. CONCLUSION

The one-dimensional finite element method compares favorably with the *in vivo* magnetic resonance data. This numerical method enables rapid prediction of flow distribution using modest computational resources. However, there are limitations that will be addressed in future work. For this experiment, we were able to specify the boundary conditions using the post-operatively measured velocity. However, this data would not be available in a true planning scenario, and methods for determining post-operative boundary conditions from pre-operative data are needed. This experiment was also sensitive to errors associated with measuring and processing the PC-MRI data. Controlled flow studies are necessary to quantify our predictive accuracy and calibrate the loss coefficients.

ACKNOWLEDGMENTS

The authors acknowledge the assistance of F. Arko, M. Draney, W.A. Lee, F. Chan, N. Pelc, C. Zarins, D. Howard, K. Wedding, A. Sawyer-Glover, W. Baumgardner, T. Brosnan, D. Parker, K. Wang, S. Spicer, and G. Chan.

REFERENCES

[1] C.A. Taylor, M.T. Draney, J.P. Ku, D. Parker, B.N. Steele, K. Wang, and C.K. Zarins, "Predictive Medicine: Computational Techniques in Therapeutic Decision-Making," *Computer Aided Surgery*, vol. 4, pp. 231-247, 1999.

[2] C.A. Taylor, T.J.R. Hughes, and C.K. Zarins, "Finite Element Modeling of Blood Flow in Arteries," *Computer Methods in Applied Mechanics and Engineering*, vol. 158, pp. 155-196, 1998.

[3] J. Wan, B.N. Steele, S. Spicer, S. Strohband, G. Feijoo, T.J.R. Hughes, and C.A. Taylor, "A One-Dimensional Finite Element Method for Simulation-Based Medical Planning for Cardiovascular Disease," *to be published in: Computer Methods in Biomechanics and Biomedical Engineering.*, 2001.

[4] N. Westerhof, F. Bosman, C.J.D. Vries, and A. Noordergraaf, "Analog Studies of the Human Systemic Arterial Tree," *Journal of Biomechanics*, vol. 2, pp. 121-143, 1969.

[5] L. Pater and J.W. van den Berg, "An Electrical Analogue of the Entire Human Circulatory System," *Med. Electron. Biol. Eng*, vol. 2, pp. 161-166, 1964.

[6] A.P. Avolio, "Multi-branched model of the human arterial system," *Medical & Biological Engineering and Computing*, vol. 18, pp. 709-718, 1980.

[7] M. Anliker, L. Rockwell, and E. Ogden, "Nonlinear Analysis of Flow Pulses and Shock Waves in Arteries," *ZAMP*, vol. 22, pp. 217-246, 1971.

[8] T.J.R. Hughes, "A Study of the One-Dimensional Theory of Arterial Pulse Propagation,". Berkeley: U. C. Berkeley, 1974.

[9] B. Hillen, H.W. Hoogstraten, and L. Post, "A Mathematical Model of the Flow in the Circle of Willis," *Journal of Biomechanics*, vol. 19, pp. 187-194, 1986.

[10] P.J. Reuderink, H.W. Hoogstraten, P. Sipkema, B. Hillen, and N. Westerhof, "Linear and Nonlinear One-Dimensional Models of Pulse Wave Transmission at High Womersley Numbers," *Journal of Biomechanics*, vol. 22, pp. 819-827, 1989.

[11] J.P. Ku, M.T. Draney, W.A. Lee, F. Arko, C.K. Zarins, and C.A. Taylor, "Comparisons of in vivo MRI flow measurements and predicted flow simulation results," presented at ASME Summer Bioengineering Conference, Snowbird, Utah, 2001.

[12] T.J.R. Hughes and J. Lubliner, "On the One-Dimensional Theory of Blood Flow in the Larger Vessels," *Mathematical Biosciences*, vol. 18, pp. 161-170, 1973.

[13] M.S. Olufsen, "A Structured Tree Outflow Condition for Blood Flow in the Larger Systemic Arteries," *American Journal of Physiology*, vol. 276, pp. H257-H268, 1999.

[14] B.R. Munsun, D.F. Young, and T.H. Okiishi, "Viscous Flow in Pipes," in *Fundamentals of Fluid Mechanics*. New York: John Wiley & Sons, 1990, pp. 504-517.

[15] B.D. Seeley and D.F. Young, "Effect of Geometry on Pressure Losses Accross Models of Arterial Stenoses," *Journal of Biomechanics*, vol. 9, pp. 439-448, 1976.

[16] D.J. Wood, L.S. Reddy, and J.E. Funk, "Modeling Pipe Networks Dominated by Junctions," *Journal of Hydraulic Engineering*, vol. 19, pp. 949-958, 1993.

[17] K.C. Wang, R.W. Dutton, and C.A. Taylor, "Level Sets for Vascular Model Construction in Computational Hemodynamics," *IEEE Engineering in Medicine and Biology*, vol. 18, pp. 33-9, 1999.

[18] N.J. Pelc, F.G. Sommer, K.C.P. Li, T.J. Brosnan, R.J. Herfkens, and D.R. Enzmann, "Quantitative Magnetic Resonance Flow Imaging," *Magnetic Resonance Quarterly*, vol. 10, pp. 125-147, 1994.